Eur. Phys. J. C 21, 513–519 (2001)
Digital Object Identifier (DOI) 10.1007/s100520100752

THE EUROPEAN PHYSICAL JOURNAL C

Scaling phenomena from non-linear evolution in high energy DIS

M. Lublinsky[a]

Department of Physics, Technion – Israel Institute of Technology, Haifa 32000, Israel

Received: 11 June 2001 / Revised version: 13 July 2001 /
Published online: 17 August 2001 –

Abstract. The numerical solutions of the non-linear evolution equation are shown to display the "geometric" scaling recently discovered in the experimental data. The phenomena hold both for proton and nucleus targets for all x below 10^{-2} and $0.25\,\mathrm{GeV}^2 \leq Q^2 \leq 2.5\times 10^3\,\mathrm{GeV}^2$. The scaling is practically exact (few percent error) in the saturation region. In addition, an approximate scaling is found in the validity domain of the linear evolution where it holds with about 10% accuracy.
Basing ourselves on the scaling phenomena we determine the saturation scale $Q_\mathrm{s}(x)$ and study both its x dependence and the atomic number dependence for the nuclei.

1 Introduction

The experimental data on the structure function F_2 were recently discovered to display the exciting phenomenon called "geometric" scaling [1]. Namely, the total $\gamma^* p$ cross section is not a function of the two independent variables x and Q, but is rather a function of the single variable $\tau = Q/Q_\mathrm{s}(x)$. The function $Q_\mathrm{s}(x)$ is a new scale called the saturation scale. The scaling holds experimentally with 10% accuracy in the whole kinematic region of $x \leq 10^{-2}$ [1].

These remarkable phenomena require theoretical explanation. In fact, the scaling behavior is actually anticipated in high density QCD and is strongly related to the appearance of the saturation scale [2–5]. During the interaction a parton cascade is developed. When the parton density (we mean the packing factor) is not large the transverse momenta of the partons are strongly ordered. Such a system evolves according to the linear DGLAP equation [6] which describes the gluon emission. As a result of this radiation the number of partons rapidly increases. However, in the high parton density phase annihilation processes become significant and they suppress the gluon radiation resulting in the saturation of the density. This scenario occurs at the saturation scale $Q_\mathrm{s}(x)$ [3,7,8], which has the meaning of the average transverse momentum of partons in the cascade. At photon virtualities below $Q_\mathrm{s}(x)$ the ordering in the momenta does not persist anymore and all partons have the same momenta $Q_\mathrm{s}(x)$. This is a domain where the evolution cannot be described by a linear equation. A non-linear evolution should be used instead. The scaling is a property of this kinematic region. It just says that the very same average momentum $Q_\mathrm{s}(x)$ in the cascade can be approached from two directions either by varying the virtuality Q at fixed x or vice versa. The scaling phenomena are expected at $Q < Q_\mathrm{s}(x)$. Furthermore, the saturation scale $Q_\mathrm{s}(x)$ can be defined as a scale at which the scaling breaks down.

As a result of the above discussion we conclude that the scaling phenomena should be a consequence of the non-linear evolution, with the non-linear effects switching on at the saturation scale. Numerous efforts to understand theoretically the mechanisms responsible for the parton saturation [3,7–13] led finally to the very same non-linear evolution equation [7,8,11–15]. A most transparent form of this equation was obtained by Kovchegov in the color dipole approach [12]:

$$\begin{aligned} &N(\boldsymbol{x_{01}}, Y; b) \\ &= N(\boldsymbol{x_{01}}, Y_0; b)\exp\left[-\frac{2C_F\alpha_\mathrm{S}}{\pi}\ln\left(\frac{\boldsymbol{x_{01}^2}}{\rho^2}\right)(Y-Y_0)\right] \\ &\quad + \frac{C_F\alpha_\mathrm{S}}{\pi^2}\int_{Y_0}^{Y}\mathrm{d}y\exp\left[-\frac{2C_F\alpha_\mathrm{S}}{\pi}\ln\left(\frac{\boldsymbol{x_{01}^2}}{\rho^2}\right)(Y-y)\right] \\ &\quad \times \int_\rho \mathrm{d}^2\boldsymbol{x_2}\frac{\boldsymbol{x_{01}^2}}{\boldsymbol{x_{02}^2 x_{12}^2}}\left(2N\left(\boldsymbol{x_{02}}, y; \boldsymbol{b}-\frac{1}{2}\boldsymbol{x}_{12}\right)\right. \\ &\quad \left. - N\left(\boldsymbol{x_{02}}, y; \boldsymbol{b}-\frac{1}{2}\boldsymbol{x}_{12}\right)N\left(\boldsymbol{x_{12}}, y; \boldsymbol{b}-\frac{1}{2}\boldsymbol{x}_{02}\right)\right) \end{aligned} \quad (1.1)$$

The equation is written for $N(r_\perp, x; b) = \mathrm{Im}a^\mathrm{el}_\mathrm{dipole}(r_\perp, x; b)$ with $a^\mathrm{el}_\mathrm{dipole}$ being the elastic amplitude for a dipole of size $r_\perp$ scattered at the impact parameter b. The rapidity $Y = -\ln x$ and $Y_0 = -\ln x_0$. The ultraviolet cutoff ρ is needed to regularize the integral, but it does not appear in physical quantities. In the large N_c limit (number of colors) $C_F = N_c/2$.

Equation (1.1) describes the following physical picture. The evolution kernel $\boldsymbol{x_{01}^2}/(\boldsymbol{x_{02}^2 x_{12}^2})$ is the probability for the dipole of size $\boldsymbol{x_{10}}$ to decay into two dipoles of sizes $\boldsymbol{x_{12}}$ and $\boldsymbol{x_{02}}$. Then these two dipoles interact independently

[a] e-mail: mal@techunix.technion.ac.il

with the target (linear term in the equation). The non-linear term in the evolution takes into account the Glauber corrections for the interaction. These corrections are due to the screening between the two dipoles, and hence they contribute with a negative sign.

It can be seen from the form of (1.1) that it contains no information about the target. The only dependence on the target is coded in the initial conditions of the evolution at some initial value x_0. We take for the initial conditions the Glauber–Mueller (GM) formula, which has been proven to be a correct initial distribution for nuclear targets [12]. For the proton target we also use the Glauber–Mueller formula. However, in this case the procedure is less justified theoretically and we rely in our choice on the fact that this formula describes well the experimental data at not too low x. The initial conditions are

$$N(\boldsymbol{x_{01}}, x_0; b) = N_{\rm GM}(\boldsymbol{x_{01}}, x_0; b), \tag{1.2}$$

with

$$N_{\rm GM}(\boldsymbol{x_{01}}, x; b) = 1 - \exp\left[-\frac{\alpha_{\rm S}\pi \boldsymbol{x_{01}^2}}{2N_c R^2} x G^{\rm DGLAP}(x, 4/\boldsymbol{x_{01}^2}) S(\boldsymbol{b})\right]. \tag{1.3}$$

Equation (1.3) takes into account the multiple dipole–target interaction in the eikonal approximation [16–18]. The gluon density $xG^{\rm DGLAP}$ is a solution of the DGLAP equation [6]. The function $S(b)$ is a dipole profile function inside the target, while R stands for its radius.

It is worth to stress that all physical results derived from the solution of (1.1) display a certain sensitivity to the initial conditions. This sensitivity dies out at very low x. Note that the unitarized form of the initial conditions (1.2) implies the existence of the saturation scale even at the beginning of the evolution ($x = x_0$). However, for our phenomenologically motivated choice for the initial conditions (1.2) and $x_0 = 10^{-2}$ the saturation scale $Q_{\rm s}(x_0)$ is much smaller than 1 GeV.

Solutions to (1.1) were studied in the asymptotic limits in [4,5]. Numerical solutions of (1.1) were reported in [15, 19–21]. We continue studying the properties of the solutions obtained in [19,21]. In the present work we concentrate on the scaling phenomena displayed by the solutions of (1.1). Indeed, it was shown in [5] that in the double logarithmic approximation, the solutions of (1.1) scale with a good accuracy in a wide high energy region. The recent paper [20] reports on the numerical observation of the scaling phenomena.

The main goal of the present paper is to discover the scaling phenomena in the solutions for both proton and nuclei obtained in the [19,21]. Basing ourselves on this property we determine the saturation scale $Q_{\rm s}(x)$ and for nuclei we study its A dependence.

This paper is organized as follows. Section 2 is devoted to the scaling phenomena and saturation scale for the proton. The scaling on nuclei is investigated in Sect. 3. The final section, Sect. 4, concludes the work.

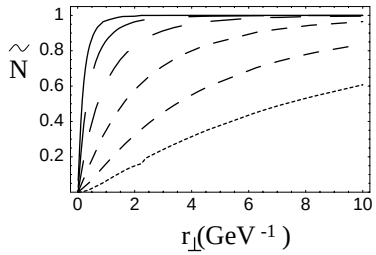

Fig. 1. Solutions of (1.1) as a function of distance. The different curves correspond to solutions at $x = 10^{-7}$ (the upper curve), 10^{-6} and so on down to $x = 10^{-2}$ (the lowest curve)

2 Scaling and saturation scale for proton

Recently [19] the non-linear evolution equation (1.1) was solved numerically for a constant value of the strong coupling constant $\alpha_{\rm S} = 0.25$. The goals of the present research are to further study the physical properties displayed by the solutions of (1.1).

Compared to [19] in the present paper we slightly modified the large distance behavior of the initial conditions at $x_0 = 10^{-2}$. In fact, no information about large distances is known. The GRV parameterization [22] entering the initial conditions ends up at distances $\simeq 0.5$ fm. In a previous paper [19] the extrapolation to larger distances was done by a constant, which does not approach unity at the very large distances. Moreover, such initial conditions cannot be consistent with a scaling that is a purely dynamical property of the evolution equation. There exists a transition region below $x = x_0 = 10^{-2}$ where the solutions of (1.1) are sensitive to the initial conditions. In this transition region we do not expect to observe any scaling phenomena. The transition region is estimated to end up at $x \simeq 10^{-4}$. Below $x \simeq 10^{-4}$ the initial conditions are forgotten and the dynamics is governed by the pure evolution. Then the scaling sets in and indeed it is seen in the solutions obtained in [19].

In order to eliminate the transition region, in the present work we extrapolate the large distance behavior of the initial conditions consistently with the asymptotics and the scaling. The following procedure can be suggested. We take a solution of [19] at some x well below the transition region, say at $x = 10^{-6}$. Appropriately rescaled this solution is used for the large distance extrapolation of the initial conditions at $x = 10^{-2}$. The above described improvement of the initial conditions modifies slightly the large distance behavior of the solution in the transition region $10^{-4} \leq x \leq 10^{-2}$ and restores the scaling in this region. Note that in a sense our procedure already implies scaling at very large distances.

The solutions obtained $\tilde{N}(r_\perp, x) \equiv N(r_\perp, x; b = 0)$ are displayed in Fig. 1. The different curves correspond to the different values of x. As can be seen from Fig. 1, at any fixed x the solution $\tilde{N}$ behaves in a step-like manner as a function of distance: at small distances it tends to zero, while at larger distances the saturation value unity is approached.

The impact parameter dependence of the function N can be restored using the following ansatz:

$$N(r_\perp, x; b) = (1 - \mathrm{e}^{-\kappa(x, r_\perp) S(b)}), \tag{2.4}$$

with

$$\kappa(x, r_\perp) = -\ln(1 - \tilde{N}(r_\perp, x)). \tag{2.5}$$

In [19] this ansatz was shown to be a quite good approximation of the exact b dependence of the solution.

2.1 Scaling phenomena

In this section we study a possible scaling behavior of the solution $\tilde{N}$. As has been mentioned, the double logarithmic approximation of the solutions of the master equation (1.1) [5] as well as general analyses of similar non-linear equations [2] predict this new scaling phenomenon in the saturation region $r_\perp > 1/Q_\mathrm{s}(x)$. In the saturation region this scaling implies the dipole–target amplitude to be a function of only one variable $\tau = r_\perp^2 \cdot Q_\mathrm{s}^2(x)$:

$$\tilde{N}(r_\perp, x) \equiv \tilde{N}(\tau). \tag{2.6}$$

Indeed, with proper rescaling of the variable $r_\perp$ all the curves in the Fig. 1 can be mapped one onto another. This is a manifestation of the scaling property (2.6).

A rigorous numerical procedure for the scaling detection can be defined. It is useful to introduce the rapidity variable $y = \ln 1/x$. Let us define the following derivative functions assuming the scaling behavior (2.6):

$$N_y(r_\perp, x) \equiv -\frac{\partial \tilde{N}}{\partial y} = \frac{\mathrm{d}\tilde{N}}{\mathrm{d}\tau} r_\perp^2 \frac{\mathrm{d}Q_\mathrm{s}^2(x)}{\mathrm{d}\ln x}, \tag{2.7}$$

$$Nr(r_\perp, x) \equiv r_\perp^2 \frac{\partial \tilde{N}}{\partial r_\perp^2} = \frac{\mathrm{d}\tilde{N}}{\mathrm{d}\tau} r_\perp^2 Q_\mathrm{s}^2(x). \tag{2.8}$$

From (2.7) and (2.8) one can see that the ratio N_y/N_r is a function of only one variable x:

$$\mathrm{Ra}(r_\perp, x) \equiv \frac{N_y}{N_r} = \frac{\mathrm{d}\ln Q_\mathrm{s}^2(x)}{\mathrm{d}\ln x}. \tag{2.9}$$

Our goal is to investigate the above ratio from the solutions obtained. In Fig. 2 the derivative functions N_r and N_y are plotted versus $r_\perp$ for various values of x. One can clearly observe a similarity in the behavior of these functions. This is actually a sign of the scaling phenomena. Both functions, N_r and N_y, possess extremum points at which the derivatives with respect to $r_\perp$ vanish. If the scaling behavior takes place then it follows from (2.6) that both N_r and N_y are extreme at the same points. In fact, this condition is clearly observed with a very good accuracy (Fig. 2).

In order to establish the scaling phenomena numerically we have to check if the function Ra is indeed $r_\perp$ independent. However, it is clear that we cannot expect exact numerical independence. So, a numerical criterion for the scaling existence has to be defined. In this paper we

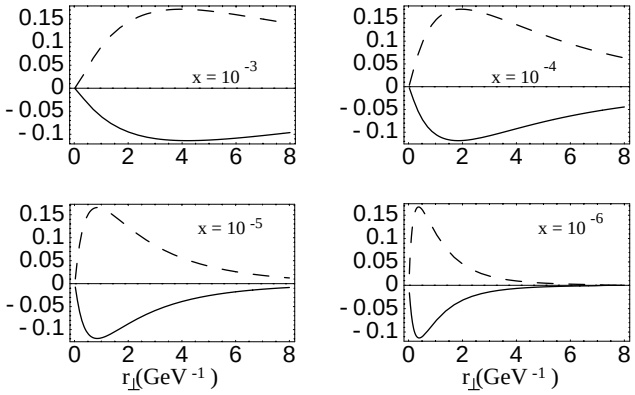

Fig. 2. The derivative functions N_r (dashed line) and N_y (solid line) as functions of the distance $r_\perp$

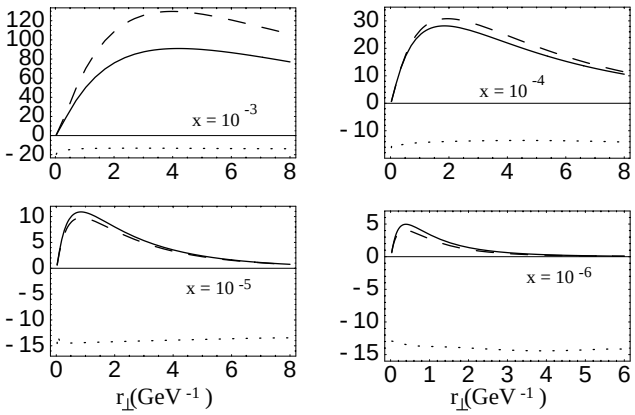

Fig. 3. The scaling as a function of the distance $r_\perp$. The positive curves are $N_r/N_{r,\min}$ (dashed line) and $N_y/N_{y,\min}$ (solid line). The dotted line is $20 \times \mathrm{Ra}$

study scaling within the distance interval $0.04\,\mathrm{GeV}^{-1} \leq r_\perp \leq 10\,\mathrm{GeV}^{-1}$ that corresponds to $0.25\,\mathrm{GeV}^2 \leq Q^2 \leq 2.5 \times 10^3\,\mathrm{GeV}^2$. Since the experimental accuracy for the scaling is about 10% we define the following condition for its acceptance:

$$\frac{\max \Delta \mathrm{Ra}}{\max \Delta N_{r,y}} \leq 10\%, \tag{2.10}$$

where $\max\Delta\mathrm{Ra}$ is a maximal variation (in percents) within the interval of interest of the function Ra with the distance $r_\perp$ at fixed x. The functions $\max\Delta N_{r,y}$ are similarly defined. The condition (2.10) says that we accept for the scaling some small $r_\perp$ dependence of the function Ra in a scale of large variations of the functions N_r and N_y.

Figure 3 presents the main results. The three lines correspond to the functions N_r and N_y divided by their minimal values within the interval, and the function Ra is multiplied by the factor 20 as can be seen on the scale.

The function Ra is clearly observed to be a very slowly varying function of $r_\perp$ for all values of x and $r_\perp$. Though at fixed x the function Ra cannot be claimed to be exactly constant; its variations with $r_\perp$ are very much suppressed compared to the variations of the functions N_r and N_y.

For example, at $x = 10^{-5}$ within the given interval the function Ra changes by a maximum of 15%. Within the very same interval both functions, N_r and N_y, change several times. Then the relative fluctuation is much less than 10%, which according to the condition (2.10) confirms the scaling. The phenomenon holds with a few percent accuracy and it improves at smaller $x \simeq 10^{-7}$ and in the deep saturation region. However, to observe this scaling behavior in these regions is numerically more problematic, since both derivatives N_r and N_y tend to zero.

As was discussed in the introduction, we should expect the scaling violation at distances of order $1/Q_s(x)$. The shorter distances are in the realm of applicability of the linear equation which is not supposed to display any scaling phenomena. Nevertheless, we observe the scaling actually to exist also at distances which are much shorter than the saturation scale. The above statements seem to contradict each other. We believe, however, that the resolution of the paradox is in the linear equation which in fact exhibits an approximate scaling behavior [5]. Unfortunately, this numerical coincident prevents us from determination of the saturation scale as a scale of the scaling violation.

2.2 Saturation scale

No exact mathematical definition of the saturation scale is known so far. In [19] two definitions of the saturation scale were proposed and the solutions obtained from (1.1) were used for its determination. For the step-like function it is natural to define the saturation scale as a position where $\tilde{N} = 1/2$:

Definition 1:

$$\tilde{N}(2/Q_s, x) = 1/2. \tag{2.11}$$

An alternative definition of the saturation scale is

Definition 2:

$$\kappa \equiv -\ln[1 - \tilde{N}(2/Q_s, x)] = 1/2. \tag{2.12}$$

The latter definition is related to the b dependence of the solution and is motivated by the GM formula with κ being the gluon packing factor[1]. This definition is equivalent to $\tilde{N}(2/Q_s, x) \simeq 0.4$ which predicts a somewhat larger saturation scale $Q_s(x)$ comparing with (2.11). The saturation scales obtained through (2.11) and (2.12) are plotted in Fig. 4a.

The saturation scale can be deduced directly from the scaling property (2.6) which has been established. To this goal we can regard (2.9) as a new definition of the saturation scale:

[1] In the present paper as well as in the previous papers [19, 21] we do not deduce the saturation scale Q_s but rather the dipole saturation radius R_s. The equality $Q_s \equiv 2/R_s$ is motivated by the double logarithmic approximation. Though for (1.1) this approximation is not justified, we still believe it to make reliable estimates provided Q_s is sufficiently large

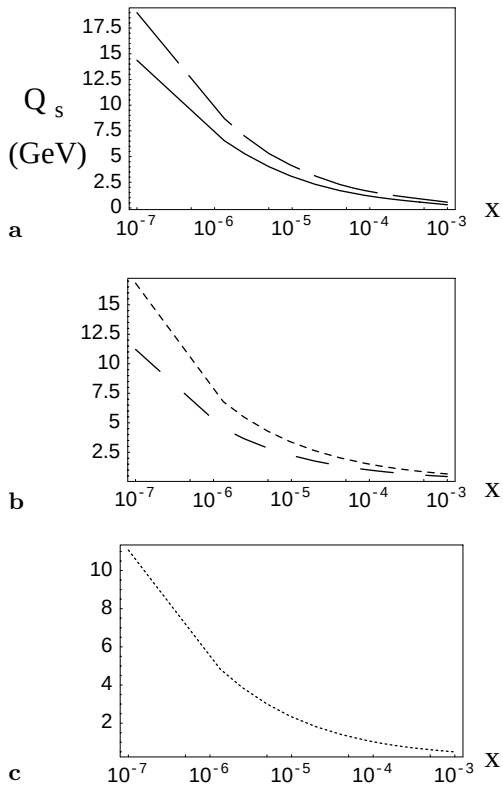

Fig. 4a–c. The saturation scale Q_s is plotted as a function of x. **a** The scales obtained from (2.11) (solid line) and (2.12) (dashed line); **b** now (2.14) is used to determine the scale. **c** The result obtained from (2.15)

Definition 3:

$$\frac{\mathrm{d}\ln Q_s^2(x)}{\mathrm{d}\ln x} = \mathrm{Ra}(r_\perp, x) = \mathrm{const}(r_\perp). \tag{2.13}$$

This definition allows us to determine the energy dependence of the saturation scale. Note from Fig. 3 that the function Ra is practically independent of x, $\mathrm{Ra} \simeq -0.7$. Hence we obtain from (2.13) the power law dependence of the saturation scale on x:

$$Q_s(x) = Q_{s0}x^{-q} = Q_{s0}\mathrm{e}^{-q\ln x}; \quad q = 0.35 \pm 0.04. \tag{2.14}$$

The obtained dependence of the saturation scale on x is somewhat weaker than both the double logarithmic prediction $q = 2\alpha_S N_c/\pi$ [5] and the numerical result of [20] but significantly stronger than the GW saturation model $q_{GW} = 0.288/2$ [23]. Unfortunately, the parameter Q_{s0} cannot be deduced from the scaling analysis only. In order to make some estimates we choose two reasonable values for Q_{s0} just fixing the saturation scale at $x = 10^{-4}$: $Q_s(10^{-4}) = 1\,\mathrm{GeV}$ and $Q_s(10^{-4}) = 1.5\,\mathrm{GeV}$. The obtained results are plotted in Fig. 4b.

The physical meaning of the scale at which both N_r and N_y are extreme is that at this scale (which is a function of x) the non-linear effects responsible for the saturation set in. Thus it is natural to suggest yet another definition of the saturation scale.

Definition 4:

$$\left(\frac{\partial^2\tilde{N}}{\partial r_\perp^2\,\partial x}\right)_{r_\perp^2=4/Q_s^2(x)} \simeq \frac{\partial}{\partial r_\perp^2}\left(r_\perp^2\frac{\partial\tilde{N}}{\partial r_\perp^2}\right)_{r_\perp^2=4/Q_s^2(x)} = 0. \tag{2.15}$$

It is important to stress that the definitions (2.13) and (2.15) are not equivalent, and no one is a consequence of any other. However, if we suppose that $\kappa \sim (r_\perp^2)^{1-\gamma}$ in analogy with the GM formula, then the two definitions (2.13) and (2.15) are equivalent.

Figure 4c shows the saturation scale $Q_s(x)$ obtained from (2.15) as a function of x. The values presented are deduced with few percent errors. Figure 4c predicts smaller saturation scales compared with the ones from Fig. 4a. This fact can be naturally explained if we suppose again that $\kappa \sim (r_\perp^2)^{1-\gamma}$. Then it is easy to show that the definition (2.15) corresponds to the condition $\kappa(x, 2/Q_s) = 1$, which implies $\tilde{N}(2/Q_s, x) = 1 - 1/e \simeq 0.63$. Hence, the saturation is obtained at larger distances.

Finally it is worth to comment on the b dependence of the saturation scale. All the results presented above are obtained for $b = 0$. It follows from the ansatz (2.4) that the b dependence of the saturation scale factorizes: $Q_s(x; b) = Q_s(x; 0) \cdot S'(b)$ with S' being a decreasing function of b. Within the assumption $\kappa \sim (r_\perp^2)^{1-\gamma}$ the function $S'(b)$ can be related to the dipole profile function $S(b)$: $S' = S^{1/2(1-\gamma)}$.

3 Scaling phenomena for nuclei

Solutions of (1.1) were obtained for nucleus targets in a recent paper [21]. All details about the solutions for the six nuclei Au_{197}, Nd_{150}, Mo_{100}, Zn_{70}, Ca_{40}, and Ne_{20} can be found there. In the present work the only modification we perform is again concerned with the large distance extrapolation of the initial conditions. To this goal we use the Glauber formula for the initial conditions. For the nucleon cross section we use the result of the previous section. This way we discover that the Glauber formula extrapolates the large distance behavior of the initial conditions consistently with both the asymptotics and scaling. The solutions obtained, $\tilde{N}_A(r_\perp, x)$, display a similar step-like behavior as in the proton case (Fig. 1).

In this section we investigate the scaling phenomena for nuclei following the very same strategy as presented above. We start from computations of the derivative functions N_{rA} and N_{yA} for the nuclei, where the subscript A stands for the atomic number of a nucleus. In fact, dependences quite similar to Figs. 2 and 3 are obtained. Figure 5 presents an example of calculations for the heaviest nucleus, Au. Since in our approach the solution for Ne is almost identical to the proton (see [21] for a discussion) the Ne nucleus displays exactly the same scaling phenomena as the proton.

The scaling on gold is observed from Fig. 5. The other nuclei display the very same phenomenon. Though for nuclei the numerical fluctuations are larger it holds within at least 10% accuracy with respect to the condition (2.10).

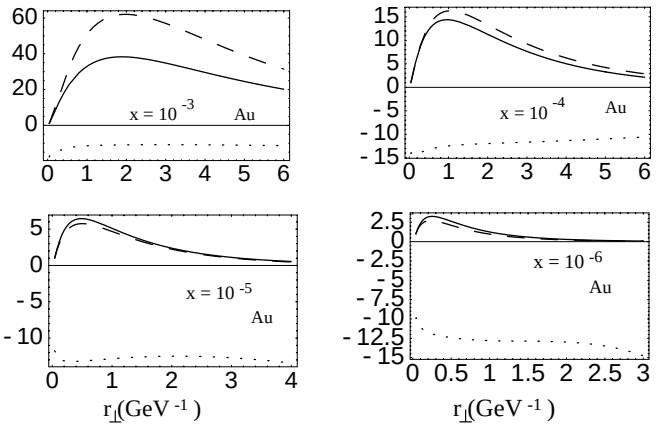

Fig. 5. The scaling as a function of distance the $r_\perp$. The positive curves are $N_{rAu}/N_{rAu,min}$ and $N_{yAu}/N_{yAu,min}$. The dotted line is $20 \times Ra_{Au}$

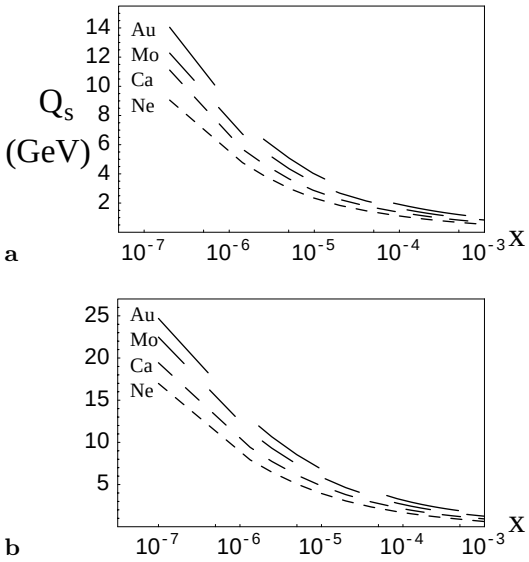

Fig. 6a,b. The saturation scale Q_s is plotted as a function of x for the four nuclei Au, Mo, Ca, and Ne. **a** This result is obtained from (2.15); **b** the result from (2.12) [21]

The ratio $Ra_A(x)$ is almost x independent, with less than 20% fluctuations. Moreover, within the same accuracy it is an A independent function as well. Recalling the definition (2.13) of the saturation scale, we obtain

$$Q_s(x) = Q_{s0}(A)x^{-q_N}; \quad q_N \simeq 0.32 \pm 0.05. \tag{3.16}$$

The power q_N is similar to the power q obtained for the proton. Note that the A dependence of the saturation scale is found to be x independent: $Q_{s0}(A) \sim A^{p_1}$, where p_1 is a constant. As was explained for the proton case, the initial values $Q_{s0}(A)$ and hence the power p_1 cannot be deduced from the scaling behavior only.

The saturation scales according to the definition (2.15) are shown in Fig. 6a for the four nuclei Au, Mo, Ca, and Ne. The numerical errors do not exceed 10%. For the sake of comparison we present in the Fig. 6b the saturation

Table 1. The power $p_2(x)$ for various values of x

Nuclei \ x	10^{-7}	10^{-6}	10^{-5}	10^{-4}	10^{-3}
Light	0.20	0.23	0.26	0.26	0.29
Heavy	0.18	0.18	0.22	0.22	0.26
All	0.19	0.20	0.23	0.23	0.27

scale obtained from (2.12) [21]. From the saturation scale obtained we can deduce its dependence on the atomic number A, where the power law $Q_{\rm s} \sim A^{p_2(x)}$ is assumed. All the nuclei are divided on two groups: light nuclei (Ne, Ca, Zn) and heavy nuclei (Zn, Mo, Nd, and Au). Table 1 presents the powers p_2 for various values of x. The relative errors in the table are estimated not to exceed 20%. On one hand, the power p_2 is seen to decrease with decreasing x. This observation agrees with the results of [21]. On the other hand, it can be deduced from Table 1 that within the errors the power $p_2(x)$ can be viewed as a constant and its average value is in a perfect agreement with the value 2/9 – the result of [20].

The scaling phenomena described above reveal themselves in the energetic gain for performing experiments on heavy nuclei. The solution for one nucleus at given x coincides with the solution for other nuclei but at different x:

$$\tilde{N}_{A_1}(r_\perp, x) \simeq \tilde{N}_{A_2}(r_\perp, \lambda(A_1, A_2)x). \qquad (3.17)$$

The coefficient λ turns out to be x independent (for example $\lambda(\mathrm{Ne}, \mathrm{Au}) \simeq 5$). The relation (3.17) is a consequence of the scaling phenomena implying $Q_{s,A_1}(x) \simeq Q_{s,A_2}(\lambda(A_1, A_2)x)$. This leads to the relation

$$\left(\frac{A_1}{A_2}\right)^{p_2} \simeq \lambda^{-q_N}. \qquad (3.18)$$

For Au and Ne this relation gives $\lambda(\mathrm{Ne}, \mathrm{Au}) \simeq 5$ in total agreement with the direct analysis of the solutions.

4 Conclusions

In the present paper the scaling phenomena in DIS were studied. The research concentrated on the non-linear evolution equation (1.1) governing the dynamics. The solutions to this equation were recently found numerically in [19] for the proton target and in [21] for the nuclei.

A criterion for the scaling based on the solution of the non-linear evolution was defined and checked numerically. For the proton we found scaling in all kinematic regions of study ($10^{-7} \le x \le 10^{-2}$, $0.25\,\mathrm{GeV}^2 \le Q^2 \le 2.5 \times 10^3\,\mathrm{GeV}^2$) and with a very good accuracy: of the order of a few percents ($\le 5\%$). The result is in agreement with the discovery of the scaling in the experimental data on the structure function F_2 [1]. The scaling behavior is predicted to improve at the LHC and THERA energies. It is important to note that scaling phenomena exist also at distances much shorter than the saturation scale [5]. At very short distances, where linear evolution occurs, no scaling should be observed. Nevertheless we found that this scaling exists numerically with about 10% accuracy and we are not able to detect its violation.

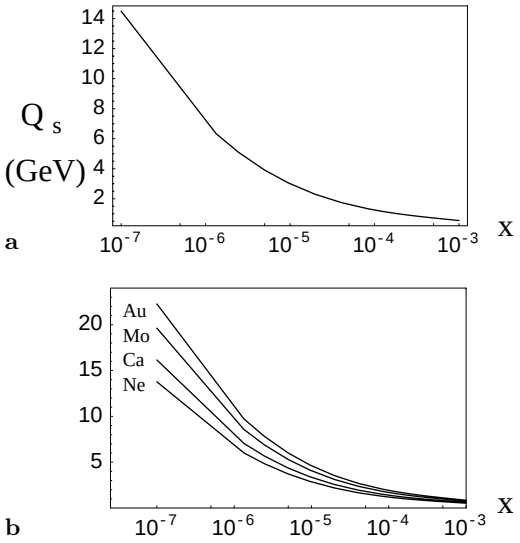

Fig. 7a,b. The average saturation scale $Q_{\rm s}$ as a function of x. **a** The result for the proton; **b** the result for the nuclei

The solution found in [19] of the non-linear equation was used to estimate the saturation scale $Q_{\rm s}(x)$. In the present work we gave two new definitions of the saturation scale based on the scaling phenomena. In spite of considerable uncertainty in the value of the saturation scale all the definitions predict that it grows with decreasing x in accordance with the theoretical expectations [3, 7–9]. If we allow ourselves to average all the results for the saturation scale depicted in Fig. 4 we would obtain the prediction shown in Fig. 7a. The relative errors for the latter are roughly 30% for all x, which indicates the uncertainty in the saturation scale definition.

The scaling phenomena were observed for the nuclear targets; these confirm the conclusions of [20]. The saturation scale estimated from the scaling displays a power law dependence on both the atomic number A and the energy variable x: $Q_{s,A}(x) \sim A^{p_2} x^{-q_N}$. The value obtained for the power p_2 is in a good agreement with the value 2/9 deduced in [20].

Both the values of the nucleus saturation scales and their A dependence obtained in the present paper are slightly different from the ones found in the [21]. The main source of this effect certainly comes from the difference in the saturation scale definitions. Since we do not know what definition is better we combine all the information we have, proceeding similarly to the proton case. The results of this procedure are presented in Fig. 7b. We hope that our predictions of the saturation scales $Q_{s,A}$ for various nuclei will serve as a theoretical basis for the RHIC data analysis in high parton density QCD [24].

Acknowledgements. I wish to thank Eugene Levin for his inspiration and support of this work. I am also very grateful to E. Gotsman, U. Maor, and K. Tuchin for illuminating discussions on the subject.

References

1. K. Golec-Biernat, J. Kwiecinski, A.M. Stasto, Phys. Rev. Lett. **86**, 596 (2001)
2. J. Bartels, E. Levin, Nucl. Phys. B **387**, 617 (1992)
3. L. McLerran, R. Venugopalan,Phys. Rev. D **49**, 2233, 3352 (1994); D **50**, 2225 (1994); D **53**, 458 (1996); D **59**, 094002 (1999)
4. Yu. Kovchegov, Phys. Rev. D **61**, 074018 (2000); E. Levin, K. Tuchin, Nucl. Phys. B **573**, 833 (2000); Non-linear evolution and saturation for heavy nuclei in DIS, hep-ph/01012175
5. E. Levin, K. Tuchin, New scaling in high energy DIS, hep-ph/0012167
6. V.N. Gribov, L.N. Lipatov, Sov. J. Nucl. Phys. **15**, 438 (1972); G. Altarelli, G. Parisi, Nucl. Phys. B **126**, 298 (1977); Yu.L. Dokshitser, Sov. Phys. JETP **46**, 641 (1977)
7. L.V. Gribov, E.M. Levin, M.G. Ryskin, Phys. Rep. **100**, 1 (1981)
8. A.H. Mueller, J. Qiu, Nucl. Phys. B **268**, 427 (1986)
9. E. Levin, M.G. Ryskin, Phys. Rep. **189**, 267 (1990); J.C. Collins, J. Kwiecinski, Nucl. Phys. B **335**, 89 (1990); J. Bartels, J. Blumlein, G. Shuler, Z. Phys. C **50**, 91 (1991); E. Laenen, E. Levin, Ann. Rev. Nucl. Part. Sci. **44**, 199 (1994) and references therein; A.L. Ayala, M.B. Gay Ducati, E.M. Levin, Nucl. Phys. B **493**, 305 (1997); B **510**, 355 (1990); Yu. Kovchegov, Phys. Rev. D **54**, 5463 (1996); D **55**, 5445 (1997); D **61**, 074018 (2000); A.H. Mueller, Nucl. Phys. B **572**, 227 (2000); B **558**, 285 (1999); Yu.V. Kovchegov, A.H. Mueller, Nucl. Phys. B **529**, 451 (1998)
10. J. Jalilian-Marian, A. Kovner, L. McLerran, H. Weigert, Phys. Rev. D **55**, 5414 (1997); J. Jalilian-Marian, A. Kovner, H. Weigert, Phys. Rev. D **59**, 014015 (1999); J. Jalilian-Marian, A. Kovner, A. Leonidov, H. Weigert, Phys. Rev. D **59**, 034007 (1999); Erratum Phys. Rev. D **59**, 099903 (1999); A. Kovner, J. Guilherme Milhano, H. Weigert, Phys. Rev. D **62**, 114005 (2000); H. Weigert, Unitarity at small Bjorken x, NORDITA-2000-34-HE, hep-ph/0004044
11. Ia. Balitsky, Nucl. Phys. B **463**, 99 (1996)
12. Yu. Kovchegov, Phys. Rev. D **60**, 034008 (2000)
13. E. Iancu, A. Leonidov, L. McLerran, Non-linear gluon evolution in the color glass condensate, BNL-NT-00/24, hep-ph/0011241; E. Iancu, L. McLerran, Saturation and universality in QCD at small x, hep-ph/0103032
14. A.H. Mueller, Nucl. Phys. B **415**, 373 (1994)
15. M. Braun, Eur. Phys. J. C **16**, 337 (2000); High energy interaction with the nucleus in the perturbative QCD with $N_c \to \infty$, hep-ph/0101070
16. A.H. Mueller, Nucl. Phys. B **335**, 115 (1990)
17. A. Zamolodchikov, B. Kopeliovich, L. Lapidus, JETP Lett. **33**, 595 (1981)
18. E.M. Levin, M.G. Ryskin, Sov. J. Nucl. Phys. **45**, 150 (1987)
19. M. Lublinsky, E. Gotsman, E. Levin, U. Maor, Non-linear evolution and parton distributions at LHC and THERA energies, hep-ph/0102321
20. N. Armesto, M. Braun, Parton densities and dipole cross sections at small x in large nuclei, hep-ph/0104038
21. E. Levin, M. Lublinsky, Parton densities and saturation scale from non-linear evolution in DIS on nuclei, Nucl. Phys. A, in press, hep-ph/01004108
22. M. Gluck, E. Reya, A. Vogt, Eur. Phys. J. C **5**, 461 (1998)
23. K. Golec-Biernat, M. Wusthoff, Phys. Rev. D **59**, 014017 (1999)
24. N. Armesto, C. Pajares, Int. J. Mod. Phys. A **15**, 2019 (2000), hep-ph/0002163; A. Krasnitz, R. Venugopalan, Phys. Rev. Lett. **86**, 1717 (2001); Nonpertubative gluodynamics of high energy heavy ion collision, hep-ph/0004116; Phys. Rev. Lett. **84**, 4309 (2000); K.J. Eskola, K. Kajantie, P.V. Ruuskanen, K. Tuominen, Nucl. Phys. **570**, 379 (2000) and references therein; K.J. Eskola, K. Kajantie, K. Tuominen, Phys. Lett. B **497**, 39 (2001); K.J. Eskola, P.V. Ruuskanen, S.S. Rasanenand, K. Tuominen, Multiplicities and transverse energies in central AA collisions at RHIC and LHC from pQCD, saturation and hydrodynamics, JYFL-3-01, hep-ph/0104010; D. Kharzeev, M. Nardi, Phys. Lett. B **507**, 121 (2001)